scientific reports

Check for updates

OPEN

Comparative genomics and biocontrol potential of five *Bacillus* strains isolated from grapevine rhizosphere

Denise M. Lajoinie[1], Ramiro Rocco Welsh[1], Constanza Rey[1], Juliet F. Nilsson[1], Andrés Martin Toscani[1], Amaru Miranda Djurhuus[2], Diego Sauka[3], Lars Hestbjerg Hansen[2], Edgardo Jofré[4] & Mariano Pistorio[1]✉

Fungal diseases such as *Botrytis cinerea* threaten grapevine production, causing substantial yield losses and quality deterioration. To manage these pathogens, viticulture relies heavily on chemical fungicides, which may negatively affect the environment, human health, and wine quality. The growing demand for environmentally safe and residue-free alternatives has therefore stimulated interest in *Bacillus* spp. as biological control agents. In this study, five *Bacillus* strains previously isolated from the rhizosphere of Argentine vineyards and known to exhibit biocontrol activity against *B. cinerea* were investigated to determine their taxonomic identity and biocontrol potential. Whole-genome sequencing and comparative genomic analyses revealed two clearly defined species groups: *Bacillus cereus sensu stricto* (FAU20, AMCV8, and TCT6) and *Bacillus subtilis sensu stricto* (AMCV2 and FAU18). The classification of *B. cereus* group strains remained challenging due to high genomic similarity and inconsistencies among current taxonomic frameworks. Genome mining identified multiple biosynthetic gene clusters associated with secondary metabolite production, including cyclic lipopeptides. Bioassays confirmed that AMCV2 and FAU18 produced cyclic lipopeptides capable of inhibiting *B. cinerea*, whereas the *B. cereus* group strains produced only siderophores. Overall, these findings support AMCV2 and FAU18 as promising candidates for sustainable *Bacillus*-based biofungicides.

Viticulture is a major global agricultural industry. However, climate change and the increasing prevalence of fungal pathogens pose growing challenges to viticulture, as rising temperatures and humidity intensify disease pressure, ultimately affecting grape quality, vineyard performance, and wine quality[1]. In recent years, global wine production has declined markedly due to extreme weather events and disease outbreaks[2]. Argentina, one of the world's leading wine-producing countries, has exceptional agroecological conditions for viticulture, with approximately 200,000 hectares of vineyards dedicated to wine and must production.

Botrytis cinerea is a necrotrophic fungus that causes gray mold and represents one of the most severe threats to wine-grape production, leading to substantial economic losses worldwide[3–6]. Grapevine cultivation demands some of the highest levels of pesticide application, as several fungal pathogens rapidly evolve to resist chemical fungicides, and their excessive use may negatively impact ecosystems and human health[5,7–9]. Calvo-Garrido et al.[10] highlight that residues of synthetic fungicides against *Botrytis* may affect not only human health but also food quality. Such residues can alter key organoleptic traits of wine (color, aroma, and flavor) by modifying phenolic and flavonoid profiles[11]. Furthermore, Esteve-Turrillas et al.[12] conducted a survey of international wines and found that nearly half of the commercial samples contained detectable levels of synthetic fungicides commonly

[1]Instituto de Biotecnología y Biología Molecular (IBBM), CCT-CONICET-La Plata, Departamento de Ciencias Biológicas, Facultad de Ciencias Exactas, Universidad Nacional de La Plata, Calles 47 y 115, La Plata 1900, Argentina. [2]Section of Microbial Ecology and Biotechnology, Department of Plant and Environmental Sciences, University of Copenhagen, 1871 Frederiksberg, Denmark. [3]Instituto de Microbiología y Zoología Agrícola (IMYZA), Instituto Nacional de Tecnología Agropecuaria (INTA), Hurlingham, Ciudad Autónoma de Buenos Aires 1686, Argentina. [4]Instituto de Biotecnología Ambiental y Salud (INBIAS), CONICET, Departamento de Ciencias Naturales, Facultad de Ciencias Exactas, Físico-Químicas y Naturales, Universidad Nacional de Río Cuarto, Río Cuarto, Argentina. ✉email: pistorio@biol.unlp.edu.ar

used against *B. cinerea*. These findings support ongoing efforts to reduce chemical inputs in viticulture through sustainable disease management strategies.

Bacillus is a genus of Gram-positive bacteria characterized by their ability to form endospores and inhabit a wide range of ecological niches[13]. In agriculture, they are known for enhancing plant tolerance to abiotic stress and serving as biological control agents against phytopathogens[14]. Some strains of *Bacillus subtilis*, commonly used as biological control agents against a wide variety of fungi, including *B. cinerea*, are Generally Recognized as Safe (GRAS)[15]. Several compounds produced by *Bacillus*, such as secondary metabolites and volatile organic compounds, are also generally considered safe for human health and the environment[16,17]. As a result, *Bacillus*-based formulations offer a promising alternative to help reduce reliance on chemical pesticides as part of integrated pest management strategies.

However, some strains, particularly those within the *Bacillus cereus sensu lato* group, are difficult to classify taxonomically[18], which can complicate their practical uses and their legislative pathway to market. This group comprises closely related lineages that differ significantly in pathogenic potential and industrial relevance. Key members of the *B. cereus* group include *B. cereus sensu stricto*, a foodborne pathogen linked to food poisoning and other infections[19,20]; *Bacillus anthracis*, the agent responsible for anthrax and a bioterrorism threat[21,22]; and *Bacillus thuringiensis*, a widely used industrial biopesticide[23,24].

In a previous study, five *Bacillus* strains isolated from the rhizosphere of Malbec and Cabernet-Sauvignon grapevine plants exhibited biocontrol activity against fungal pathogens, such as *B. cinerea* and *Alternaria alternata*[25]. The objective of this study was to determine the taxonomic identity of five previously isolated *Bacillus* strains and to characterize their phylogenomic relationships and biosynthetic potential. We further assessed whether the predicted secondary metabolites are produced and evaluated their contribution to biocontrol activity.

Results and discussion

Whole genome sequencing, assembling and annotation

In a previous study, five *Bacillus* strains (FAU18, AMCV2, FAU20, TCT6 and AMCV8) were isolated from argentinian grapevine rhizospheres and found to inhibit the growth of important fungal pathogens[25]. AMCV2 and FAU18 significantly reduced the growth of *B. cinerea*, *A. alternata*, *Fusarium oxysporum*, and *Fusarium graminearum*, with AMCV2 also inhibiting *Penicillium oxalicum*. In contrast, AMCV8, TCT6, and FAU20 exhibited narrower activity, restricting their inhibition to *B. cinerea and A. alternata*.

To gain deeper insights into the mechanisms underlying their biocontrol effects and to accurately classify these strains, the five genomes were sequenced and then assembled. Oxford Nanopore long-read datasets were evaluated using NanoPlot[26] to assess sequencing depth and read length distribution. The total number of bases sequenced ranged from 63.3 Mb (AMCV8) to 290.8 Mb (FAU18), corresponding to estimated long-read coverages between 11× and 69× (Table 1). Mean read lengths ranged from 2,413 bp (FAU20) to 3,059 bp (AMCV8 and FAU18), with read N50 values between 3,671 bp and 6,225 bp. Lower sequencing depth in AMCV8 and AMCV2 (11× and 19×, respectively), together with moderate read length distributions across datasets, likely contributed to the variability observed in assembly contiguity. All genomes displayed 100% completeness, supporting the overall quality of the assemblies despite differences in contiguity. The annotation was generated with Prokka[27], RAST[28] and eggNOG[29]. The statistics of the Prokka annotation are shown in Table 1.

The assembled genomes showed notable variation in G + C content, genome size, coding sequences (CDS), rRNA, and tRNA, with a clear distinction between TCT6, AMCV8, and FAU20, and AMCV2 and FAU18. TCT6, AMCV8, and FAU20 exhibited a G + C content of approximately 35% and genome sizes ranging from 5.5 to 5.9 Mbp, which are consistent with values commonly reported for members of the *B. cereus* group, along with a corresponding variation in CDS count[30]. The values exhibited for AMCV2 and FAU18, however, displayed features more consistent with *B. subtilis* group species, where the G + C content typically ranges between 43 and 46% and the genome sizes often range around 3.9 to 4.6 Mb[31]. The number of contigs varied between 3 and 64, with FAU18 and AMCV2 showing the highest assembly continuity. Ribosomal and transfer RNA genes were

	TCT6	AMCV8	FAU20	AMCV2	FAU18
Total bases sequenced	333,693,375	63,338,716	247,625,216	110,575,354	290,854,727
Coverage	56	11	60	19	69
Mean read length	2,855.60	3,059.40	2,413.30	2,814.10	3,050.60
Read length N50	4,547	6,225	3,671	5,128	4,999
Completeness	100%	100%	100%	100%	100%
GC%	35.0	35.0	35.2	43.8	43.7
Contigs	8	64	29	3	5
Bases	5,925,164	5,619,124	5,580,094	4,094,482	4,212,652
CDS	5,883	5,751	5,629	4,056	4,212
rRNA	39	21	30	30	30
tRNA	95	88	97	86	97
tmRNA	1	1	1	1	1

Table 1. Genome annotation statistics of the five *Bacillus* strains of interest generated with Prokka.

detected in all strains, with rRNA ranging from 21 to 39 and tRNA from 86 to 97. A single tmRNA gene was identified in each genome.

When analyzing the genome annotation performed with RAST, distinct metabolic patterns emerged that also divided the strains into two groups. The complete subsystem graphic can be found in Supplementary Fig. 1. While each strain displayed unique subsystem coverage, TCT6, AMCV8, and FAU20 showed slightly a lower proportion of annotated subsystems relative to total CDS (22–23%) compared to AMCV2 and FAU18 (28–29%). As shown in Fig. 1, the most abundant subsystems across all strains were *Amino Acids and Derivatives*, *Carbohydrates*, and *Protein Metabolism*. The grouping pattern remained evident across both highly and sparsely represented categories. For example, in *Motility and Chemotaxis*, TCT6, AMCV8, and FAU20 consistently displayed fewer associated genes than AMCV2 and FAU18.

Conversely, in other categories such as *Amino Acids and Derivatives*, or *Virulence, Disease and Defense*, TCT6, AMCV8, and FAU20 contained more annotated genes than AMCV2 and FAU18. To further investigate these patterns, we compared the annotation obtained with RAST to the generated with eggNOG, which classifies genes into Clusters of Orthologous Groups (COGs) (Supplementary Fig. 2). Unlike RAST, which organizes CDSs into functional subsystems, the COG framework is based on groups of orthologous genes that share evolutionary conserved functions. Several analogous functional categories revealed comparable grouping patterns between the strains, while others showed the inverse trend. For example, in the category of *Energy production and conversion* (COG C, corresponding to *Respiration* in RAST), TCT6, AMCV8, and FAU20 displayed slightly lower proportions than AMCV2 and FAU18. This contrasts with the RAST annotation, where TCT6, AMCV8, and FAU20 showed a higher representation of genes associated with respiration. In *Inorganic ion transport and metabolism* (COG P, analogous to *Iron acquisition and metabolism* and *Phosphorus metabolism* in RAST), the separation of the two groups was again evident, with TCT6, AMCV8, and FAU20 showing lower values than AMCV2 and FAU18, opposite to what was observed in the RAST analysis. Taken together, these patterns indicate that although the annotation frameworks are based on different principles, both RAST subsystems and eggNOG COGs capture the same underlying division of the strains into two groups.

To complement the functional annotation, a screening for antibiotic resistance genes was performed using ABRicate Galaxy Australia version 1.0.1[27,32]. Only a few resistance-associated genes were identified across the five genomes, all displaying coverage and identity values above 90%. AMCV2 and FAU18 carried *mph(K)* and *aadK*, associated with macrolide (spiramycin, telithromycin) and aminoglycoside (streptomycin) resistance, respectively. A gene conferring resistance to fosfomycin, *fosB1*, was detected in TCT6, AMCV8, and FAU20, while *blaZ*, encoding a β-lactamase was present in TCT6 (two copies) and AMCV8. Their distribution followed the same grouping pattern observed in the general genome annotation.

The presence of prophage sequences and insertion sequences (IS) was analyzed to characterize the genomic composition of the strains. ISs were identified using ISEScan Galaxy Europe version 1.7.3[33], revealing a heterogeneous distribution across the five *Bacillus* genomes. A total of 84 IS elements belonging to seven families were detected, with the most abundant being IS3, IS4, and IS21. TCT6, AMCV8, and FAU20 harbored 31, 29 and 15 IS elements, whereas the AMCV2 and FAU18 contained only 4 and 5 respectively. This reduced IS content is consistent with genomic features commonly reported for members of the *B. subtilis* group and

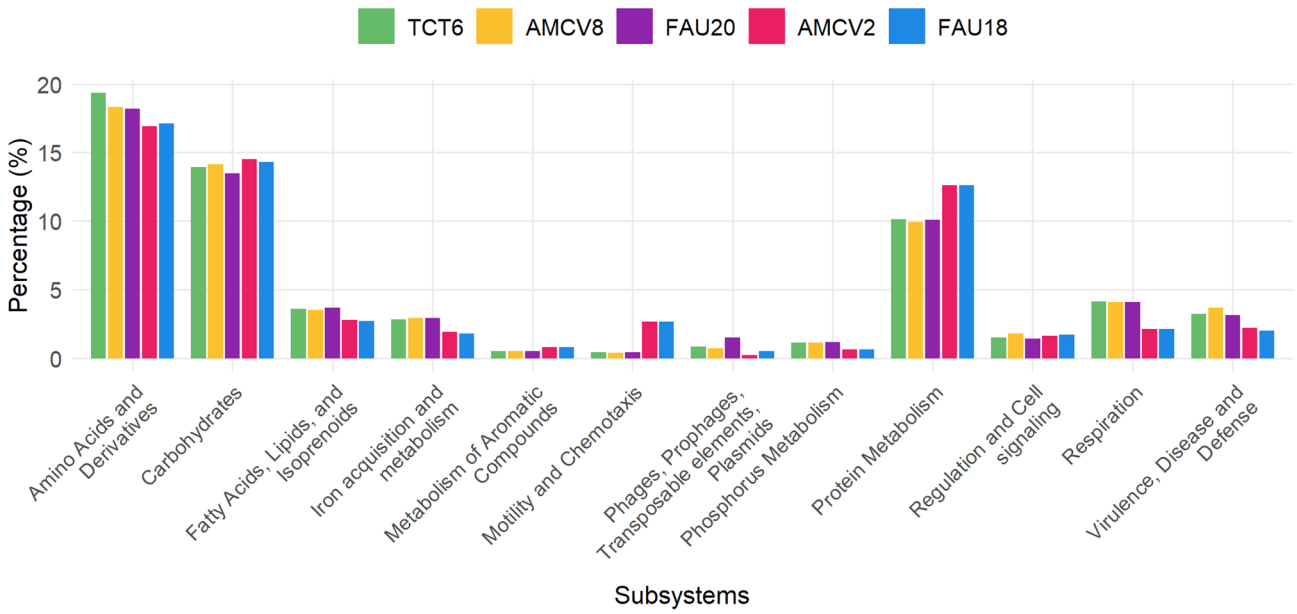

Fig. 1. Distribution of the most relevant functional subsystems annotated by RAST in the genomes of the five *Bacillus strains* (TCT6, AMCV8, FAU20, AMCV2, and FAU18). The relative abundance of each category is expressed as a percentage of the total predicted coding sequences for each strain. The complete subsystem graphic can be found in supplementary material.

was further supported by the analysis of representative reference genomes, which displayed similarly low IS counts. Conversely, the higher IS abundance observed in the other three strains is in line with patterns typically described for strains associated with the *B. cereus* group, reflecting the increased genome plasticity characteristic of this lineage.

Despite the high IS counts obtained for TCT6, AMCV8 and FAU20, pairwise ISCompare[34] analyses revealed contrasting patterns of IS relocation across conserved genomic contexts. No differentially located IS (DLIS) were detected between TCT6 and AMCV8, indicating a highly conserved IS landscape and stable IS positioning between these two genomes. In contrast, comparisons involving FAU20 (AMCV8 vs. FAU20 and TCT6 vs. FAU20) identified multiple DLIS events affecting mainly intergenic regions and, in some cases, small CDS (intragenic insertions). This supports a conserved IS repertoire and stable IS positioning in TCT6 and AMCV8, with FAU20 displaying a distinct history of IS relocation. Although AMCV2 and FAU18 harbored only a few IS elements, ISCompare nonetheless detected DLIS candidates between them, indicating differences in IS identity and/or genomic location even within a low-IS background.

Prophage sequences were identified using PHASTER[35] and Phigaro[36]. PHASTER detected between four and eight prophage regions per genome across the five *Bacillus* strains, with four regions in AMCV2 and AMCV8, five in TCT6, six in FAU18, and eight in FAU20. Each genome contained one region classified as "intact" (score > 90), except for AMCV8, in which no "intact" prophage was detected. BLASTn comparison of the "intact" prophage regions, including ± 5 kb of flanking genomic sequence, revealed that the prophages identified in AMCV2 and FAU18 exhibit very high nucleotide identity and nearly complete query coverage, indicating that these two strains carry a likely identical prophage variant inserted at the same genomic position. In contrast, intact prophages from the remaining strains showed low sequence similarity in pairwise comparisons, suggesting that they represent distinct elements.

As for "questionable" prophages (scores = 70–90) two were identified in FAU20, and one each in AMCV8 and FAU18, while none were found in TCT6 or AMCV2. "Incomplete" prophages (scores < 70) were the most abundant category, with five regions detected in FAU20, four in TCT6 and FAU18, and three in AMCV2 and AMCV8. In contrast, Phigaro predicted a total of 15 prophage regions across the five genomes, ranging from one to five per strain. The number of prophages detected per genome was one in AMCV2, two in AMCV8, three in FAU18, five in FAU20, and four in TCT6. All regions were classified as non-transposable and assigned to the families *Siphoviridae*, *Myoviridae* or Unknown. Notably, prophage regions classified as "intact" by PHASTER were consistently detected by Phigaro, indicating concordant identification of conserved prophage elements by both tools.

Overall, the combined analysis of IS and prophage elements revealed group-specific patterns of mobile genetic element distribution that are consistent with the phylogenetic relationships among the analyzed strains, highlighting both conserved and strain-specific features within each *Bacillus* lineage.

The genomes were further screened for genes associated with plant growth–promoting (PGP) traits commonly reported in *Bacillus* spp. using PLaBAse PGPT-Pred v1.02[37]. A substantial number of BLASTp/HMM-based hits were classified as "possible genes associated to PGPTs" in all five strains, with TCT6 harboring 3039, AMCV8 2974, FAU20 2847, AMCV2 2495, and FAU18 2498.

A targeted inspection of phytohormone-related traits revealed the presence of PGPT-classified genes associated with auxin (IAA) biosynthesis. In AMCV2 and FAU18, sequences corresponding to *aldH* and *ysnE* were identified, whereas TCT6, AMCV8, and FAU20 carried sequences corresponding to *ipdC* and *aldH*. No PGPT-classified hits corresponding to *iaaM*/*iaaH* were detected[38,39]. KEGG-based pathway reconstruction using GhostKOALA v3.1[40] and the KEGG Mapper Reconstruct tool (accessed February 2026)[41,42] did not support the presence of a complete canonical auxin biosynthetic pathway.

Similarly, PGPT-classified genes related to cytokinin metabolism and biosynthesis, including *ipt*, *miaA*, and *log*[43], were detected across all five genomes. However, KEGG pathway reconstruction did not support a complete canonical cytokinin biosynthetic pathway.

In contrast, no PGPT-classified genes related to gibberellin metabolism and biosynthesis[44] or to *acdS* (ACC deaminase)[45] were identified in any of the strains.

Overall, these findings suggest that although several genes associated with phytohormone-related functions are present, canonical biosynthetic pathways appear incomplete at the genomic level, and functional hormone production therefore requires experimental validation.

Phylogenetic analysis

The genus *Bacillus* encompasses a wide variety of species, some of which are pathogenic to humans. Therefore, it is crucial to accurately identify the strains in order to determine the appropriate biosafety level for handling and, in our case, to ensure their safety for potential use as biocontrol agents.

The strains were initially classified using MALDI-TOF MS, which provided genus level identification[25] thereby requiring a more refined classification. Given the genetic diversity within the *Bacillus* genus, applying multiple classification methods allows for more robust identification, helping resolve any ambiguities. As shown in Table 2, several classification approaches, such as MALDI, BTyper3[46], JSPECIES[47] and TYGS[48], were employed.

MALDI-TOF identified TCT6 as *B. thuringiensis* while AMCV8 and FAU20 were classified as *B. cereus*. BTyper3 version 3.4.0 placed them within *B. cereus sensu stricto*, while JSpecies and TYGS associated them with reference strains from both *B. thuringiensis* and *B. cereus*, depending on the tool. TYGS suggested they may represent potential new species within the *B. cereus* group. In contrast, AMCV2 and FAU18 were consistently classified as *B. subtilis* by all tools employed, except for BTyper3. This is expected, since BTyper3 is specifically designed for genotyping members of the *B. cereus* group, and therefore does not classify *B. subtilis* strains. It all suggests that AMCV2 and FAU18 may belong to the *B. subtilis sensu lato* group. Members of this group include *B. subtilis sensu stricto*, *Bacillus pumilus*, *Bacillus amyloliquefaciens*, *Bacillus licheniformis*, and other subspecies

	TCT6	AMCV8	FAU20	AMCV2	FAU18
MALDI Classification	*B. thuringiensis*	*B. cereus*	*B. cereus*	*B. subtilis*	*B. subtilis*
BTyper3 classification ANI	*B. cereus s.s.*	*B. cereus s.s.*	*B. cereus s.s.*	–	–
BTyper3 closest type strain	*B. thuringiensis serovar berliner ATCC 10,792*	*B. thuringiensis serovar berliner ATCC 10,792*	*B. cereus ATCC 14,579*	–	–
JSPECIES classification	*B. cereus str. Schrouff*	*B. cereus str. Schrouff*	*B. thuringiensis BMB171*	*B. subtilis UD1022*	*B. subtilis BEST7003*
TYGS classification	Potential new species	Potential new species	Potential new species	Belongs to known species	Belongs to known species
TYGS closest specie	*B. thuringiensis ATCC 10,792*	*B. thuringiensis ATCC 10,792*	*B. cereus ATCC 14,579*	*B. subtilis ATCC 6051*	*B. subtilis ATCC 6051*

Table 2. Classification results for the five *Bacillus* strains based on multiple methods: MALDI, BTyper3, JSPECIES, and TYGS.

derived from them[49]. To further confirm this classification, an Average Nucleotide Identity (ANI) analysis was performed, and a Phylogenetic Tree was constructed (Fig. 2).

The ANI values in the Top Fig. 2 for FAU18 and AMCV2 were highest against *B. subtilis subsp. subtilis* 168, consistently exceeding 97%. The values remain well above the ≥ threshold, supporting the classification of FAU18 and AMCV2 as *B. subtilis sensu stricto*. The phylogenetic tree in the bottom part of Fig. 2 shows FAU18 and AMCV2 clustering tightly with *B. subtilis* subsp. *subtilis* 168, clearly separated from other members of the *B. subtilis* species complex, such as *B. amyloliquefaciens*, *B. velezensis*, and *B. licheniformis*. With these results, AMCV2 and FAU18 can be classified as *B. subtilis sensu stricto*.

As for the three remaining strains, Table 2 shows their classification was less consistent since no consensus was reached even when working with multiple tools. To resolve these ambiguities, two complementary classification frameworks have been proposed. Torres Manno et al.,[50] developed a system to distinguish genomospecies within the *B. cereus* group using core-genome phylogenetic analysis combined with ANI calculations, applying a threshold of 97.09% to define genomospecies objectively. Their method focuses on genomic similarity and captures subtle evolutionary differences to build a clear, consistent taxonomy. In parallel, Carroll et al.[51] proposed a standardized nomenclature system designed particularly for applied settings. Recognizing the limitations of current species boundaries, such as the inability to reliably distinguish between *B. anthracis* and neighboring lineages, they suggest lowering the ANI threshold to 92.5%. This adjustment significantly reduces overlap between genomospecies clusters, enhancing the resolution of species-level assignments. To classify these strains, both frameworks were applied in parallel. ANI values were calculated against the reference strains proposed by Torres Manno et al.[50] and against the panel of strains suggested by Carroll et al.[51]. This dual approach enabled comparison of how each framework classified TCT6, AMCV8, and FAU20, and whether the resulting assignments were consistent or divergent.

Supplementary Fig. 3 shows the ANI heatmap constructed following the classification framework proposed by Torres Manno et al.[50]. Focusing specifically on the three isolates of interest, the highest ANI values (~ 95–96%) were observed in comparisons with *B. thuringiensis* serovar berliner ATCC 10,792 and *B. cereus* ATCC 14,579. These values indicate a high degree of genomic similarity but remain below the 97.09% threshold established to delineate genomospecies. Therefore, none of the three strains can be confidently assigned to an existing genomospecies under this framework. Figure 3 presents the ANI results using the panel of strains proposed by Carroll et al.[51]. Here, TCT6, AMCV8, and FAU20 showed ANI values of ~ 95–96% with *B. thuringiensis* serovar berliner ATCC 10,792 and *B. cereus* ATCC 14,579, exceeding the 92.5% ANI threshold defined by Carroll et al.[51], whereas all other comparisons yielded values below 92%. Based on this framework, the three strains can be placed within the *B. cereus sensu lato cluster*, but they cannot be assigned unambiguously to either *B. cereus sensu stricto or B. thuringiensis.* Importantly, in both frameworks, ANI values against *B. anthracis* were below the species-level thresholds, excluding affiliation with this species. Consistently, BTyper3 analysis did not identify major virulence determinants associated with anthrax or emetic toxin production in any of the analyzed genomes. However, the *nheABC* and *hblABCD* enterotoxin operons, as well as *cytK*-2 and the sphingomyelinase gene (*sph*), were identified, representing the typical diarrheal toxin repertoire described for *B. cereus sensu stricto*[19]. Importantly, the presence of these genes alone does not imply pathogenicity, as their expression and the environmental conditions required for toxin production were not evaluated in this study.

Taken together, these results illustrate the limitations of ANI-based classification within the *B. cereus sensu lato* group. While Torres Manno's framework leaves the strains unassigned because they do not meet the 97.09% cutoff, Carroll's framework allows their placement within the *B. cereus* cluster but without finer resolution. *B. thuringiensis* strains are historically distinguished by the production of parasporal crystal inclusions composed of crystal (Cry or Cyt) proteins. Using BTyper3, no *cry* or *cyt* crystal protein genes were detected with sufficient identity to known *B. thuringiensis* toxins. To further assess the presence of a Bt-like crystal phenotype, sporulated cultures were examined by phase-contrast microscopy[52]. After microscopic examination, no parasporal crystal inclusions were detected, indicating the absence of crystal-forming proteins. Based on this phenotypic evidence, strains FAU20, AMCV8, and TCT6 can be classified as *B. cereus sensu stricto.*

Secondary metabolite profiling for biocontrol potential

Secondary metabolites play a crucial role in the biocontrol activity of bacteria, particularly in combating plant pathogens such as *B. cinerea* and other fungal threats to grapevines[49,53]. Secondary metabolite profiles of *B.*

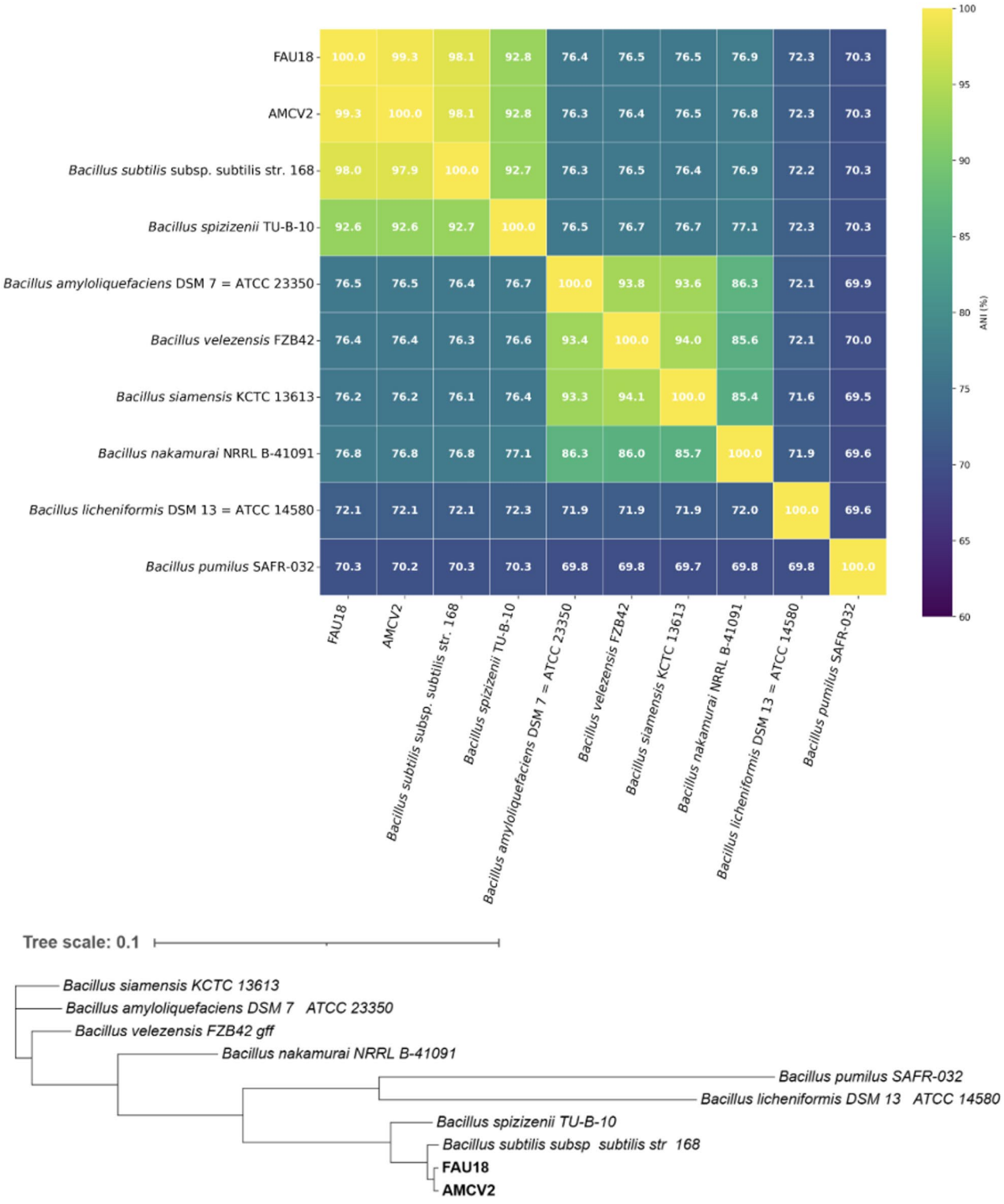

Fig. 2. Taxonomic classification of strains AMCV2 and FAU18. Top: ANI Heatmap of *Bacillus subtilis* group strains alongside AMCV2 and FAU18. The yellow-blue spectrum represents the level of similarity between the strains, with yellow indicating higher genomic similarity and blue indicating greater divergence. Bottom: Core genome phylogenetic tree of *B. subtilis* type strains including AMCV2, and FAU18.

subtilis and *B. cereus* strains were analyzed using AntiSMASH, revealing several bioactive compounds with potential antimicrobial properties.

The genome mining of TCT6 revealed the presence of 15 biosynthetic gene clusters (BGCs) belonging to diverse classes, including nonribosomal peptide synthetases (NRPS), ribosomally synthesized and post-

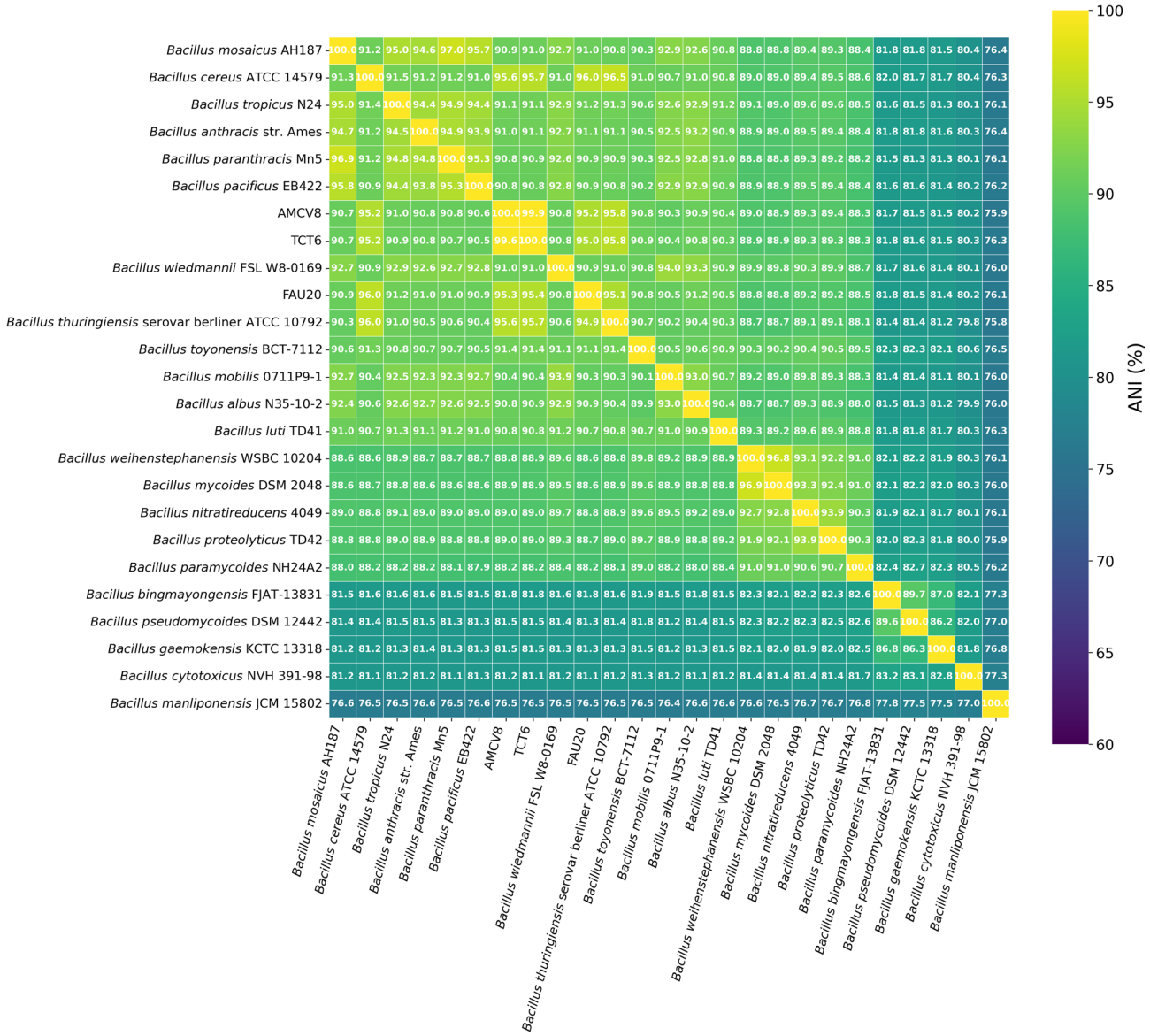

Fig. 3. ANI Heatmap of members of the *Bacillus cereus* group according to Carroll et al. (2020) alongside strains FAU20, TCT6, and AMCV8. The yellow-blue spectrum represents the level of similarity between the strains, with yellow indicating higher genomic similarity and blue indicating greater divergence.

translationally modified peptides (RiPPs), siderophores, polyketides, and terpenes. Among them, a siderophore cluster with 100% similarity to petrobactin and another with 85% similarity to bacillibactin were identified, both of which are well-known iron chelators that enhance bacterial competitiveness in iron-limited environments such as the rhizosphere[54,55]. Additionally, an NRPS cluster showed 40% similarity to fengycin, a lipopeptide with strong antifungal properties against phytopathogens, including *B. cinerea*[56]. AntiSMASH predicted 12 BGCs in the genome of AMCV8, including siderophore clusters with 100% similarity to petrobactin and 85% similarity to bacillibactin, as well as an NRPS cluster with 40% similarity to fengycin. In FAU20, 13 BGCs were identified, and among the most relevant clusters, a siderophore region with 100% similarity to petrobactin and an NRPS-metallophore cluster with 85% similarity to bacillibactin were detected again. In addition, an NRPS cluster displayed 40% similarity to fengycin.

Finally, in both AMCV2 and FAU18 AntiSMASH analysis predicted 10 BGCs, displaying an identical secondary metabolite repertoire. The clusters comprised NRPS, polyketide, RiPP, siderophore, terpene, and a T3PKS (type III polyketide synthase). Both strains carried NRPS clusters with 100% similarity to fengycin and 82% similarity to surfactin, two lipopeptides known for their antifungal and biofilm-modulating activity[57]. A siderophore cluster with 100% similarity to bacillibactin was also present. Additionally, RiPP clusters corresponding to subtilosin A and bacilysin (both 100% similarity) were identified, providing further antimicrobial potential.

Given the known biocontrol potential of the five *Bacillus* strains, many of the secondary metabolites identified through antiSMASH could be responsible for their antagonistic activity against *B. cinerea* and other grapevine pathogens. Since all five strains carried BGCs associated with lipopeptide biosynthesis, particular attention was given to this metabolite class due to its well-documented role in fungal antagonism. *Bacillus* species are known producers of cyclic lipopeptides such as surfactin, fengycin, and iturin, which contribute to biocontrol activity via diverse mechanism[17,56,58]. Taken together, the AntiSMASH analyses highlighted AMCV2 and FAU18 as the strains with the strongest genetic evidence for lipopeptide biosynthesis.

Comparative analysis of biosynthetic gene clusters of interest

Given that AntiSMASH predicted biosynthetic gene clusters with high similarity to known compounds (namely bacillibactin in all five strains, petrobactin in the three *B. cereus s.s* strains, and fengycin in the two *B. subtilis s.s.* strains) a comparative analysis was performed to assess the degree of conservation of these clusters among the strains. This analysis aimed to determine whether the corresponding biosynthetic gene clusters shared similar gene content and organization, thereby indicating conserved biosynthetic potential.

The fengycin biosynthetic gene clusters predicted in AMCV2 and FAU18 were compared at the protein and synteny levels. BLASTp analysis revealed high amino acid identity across the entire cluster (95.4% identity with 100% query coverage). In addition, synteny analysis performed with Clinker[59] confirmed identical gene organization and orientation between both strains, indicating a highly conserved fengycin biosynthetic gene cluster (Supplementary Fig. 4A).

Comparative analysis of the petrobactin biosynthetic gene clusters from strains TCT6, AMCV8, and FAU20 with BLASTp revealed high amino acid identity (96–99%) across homologous regions, however, this similarity was restricted to partial sequence coverage (~ 32–34%). Synteny analysis showed conservation of a central biosynthetic region shared by all three strains, with TCT6 and AMCV8 displaying a more similar gene organization, whereas FAU20 exhibited a slight divergence (Supplementary Fig. 4B). These observations indicate conservation of the petrobactin biosynthetic machinery, accompanied by strain-specific variation rather than complete cluster conservation.

Finally, comparative analysis of the bacillibactin biosynthetic gene clusters revealed distinct conservation patterns among the analyzed strains. In AMCV2 and FAU18, BLASTp comparisons showed near-complete similarity (98.4% amino acid identity over 87% query coverage), which was further supported by synteny analysis demonstrating highly conserved gene order and organization (Supplementary Fig. 4C). These results indicate a strongly conserved bacillibactin biosynthetic machinery in these two closely related strains.

In contrast, bacillibactin-associated clusters in TCT6, AMCV8, and FAU20 exhibited high amino acid identity (95–97%) but limited query coverage (~ 41–44%), suggesting conservation of core NRPS domains but divergence at the cluster level. Synteny analysis confirmed the presence of a shared central biosynthetic region;

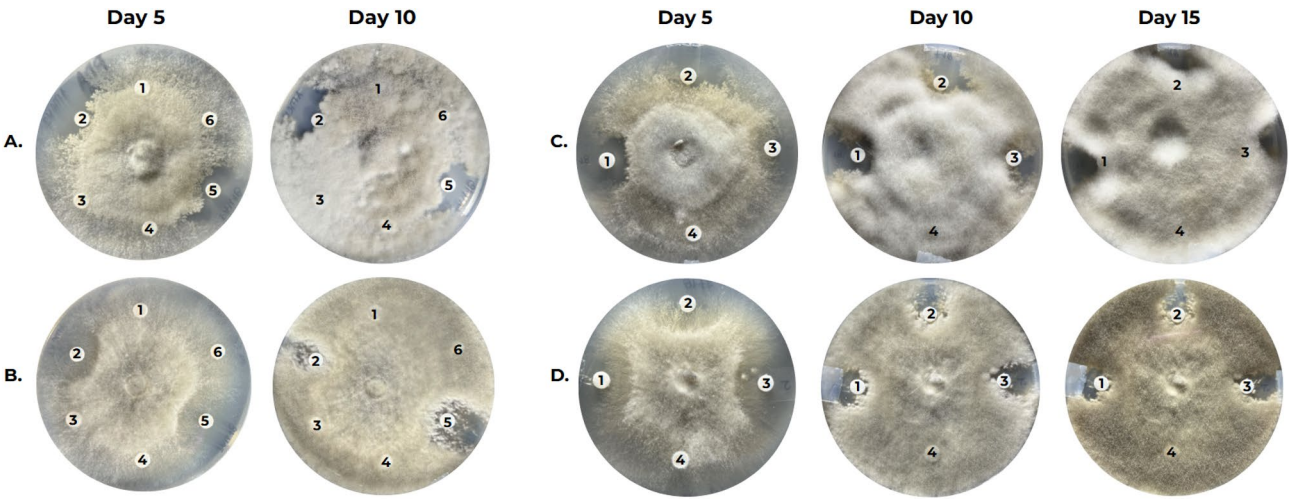

Fig. 4. Antifungal activity of *Bacillus* lipopeptides against *Botrytis cinerea*. Mycelial transplant assay. The figure shows an agar plug of **A**. *B. cinerea* B05.10 mycelium and **B.** *B. cinerea* T4 in the center of a PDA Petri dish, and discs impregnated with purified lipopeptides from the five *Bacillus* strains and a methanol impregnated disc that serves as a negative control are positioned equidistantly at ~ 3 cm from the plug. Numbers on the plate indicate disc positions: 1 = Negative control, 2 = *B. subtilis s.s.* AMCV2, 3 = *B. cereus s.s.* TCT6, 4 = *B. cereus s.s.* AMCV8, 5 = *B. subtilis s.s.* FAU18, 6 = *B. cereus s.s.* FAU20. Synergy assay of lipopeptides from *B. subtilis s.s.* AMCV2 and *B. subtilis s.s.* FAU18 against *Botrytis cinerea*. A mycelial plug of **C**. *B. cinerea* 05.10 and **D**. *B. cinerea* T4 is in the center of the PDA Petri dish. Discs impregnated with purified lipopeptides are positioned equidistantly at ~ 3 cm from the plug. Numbers on the plate indicate disc positions: 1 = *B. subtilis s.s.* FAU18 (20 µL), 2 = *B. subtilis s.s.* AMCV2 + *B. subtilis s.s.* FAU18 (10 µL each), 3 = *B. subtilis s.s.* AMCV2 (20 µL), 4 = methanol (20 µL, negative control). Images were taken after 5, 10 and 15 days of incubation at 25 °C.

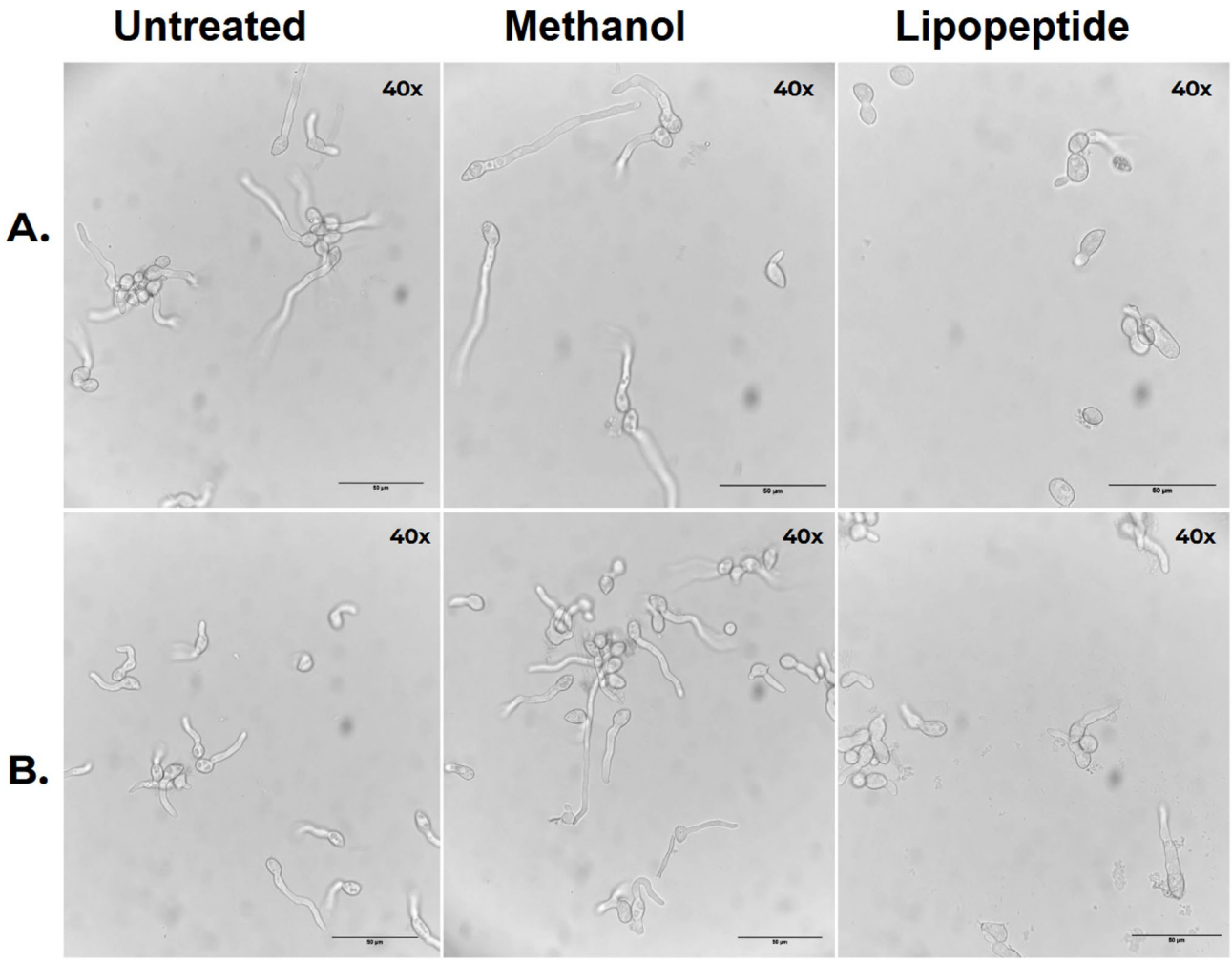

Fig. 5. Effect of lipopeptides from A. *B. subtilis s.s.* AMCV2 and B. *B. subtilis s.s.* FAU18 on conidial germination of *Botrytis cinerea* B05.10 after 6 h of incubation.

however, TCT6 and AMCV8 displayed a more similar cluster organization, whereas FAU20 showed additional differences in flanking regions. This pattern reflects conservation of essential biosynthetic functions embedded within a variable genomic context. It is important to note that all analyses were performed on draft genome assemblies comprising multiple contigs rather than complete, closed genomes. Consequently, some apparent structural divergences, particularly in large NRPS-encoding clusters such as fengycin and bacillibactin, may reflect assembly fragmentation or contig boundary effects rather than true biological differences. This limitation is especially relevant for large modular enzymes, whose extensive repetitive domains can complicate assembly resolution. Therefore, while the observed conservation patterns are robust at the protein level, structural variations at the cluster level should be interpreted with caution.

Isolation and antifungal activity of cyclic lipopeptides

To further investigate the mechanisms underlying the observed biocontrol activity, lipopeptides were precipitated from the culture supernatants of the five *Bacillus* strains and tested for antifungal activity against *B. cinerea* through mycelial plug-disc diffusion assays (Fig. 4). A mycelial plug was taken from an actively growing *B. cinerea* culture and transferred onto a fresh PDA plate. Paper discs impregnated with lipopeptides from each *Bacillus* strain, along with a methanol-impregnated disc serving as a negative control, were positioned approximately 3 cm from the fungal plug. After 20 days of incubation, only AMCV2 and FAU18 produced clear inhibition zones around the discs, while TCT6, AMCV8, and FAU20 showed no visible inhibitory effect. The methanol control did not affect fungal growth, confirming the solvent was not responsible for the observed activity. Figure 4A and B present the results obtained after 5 and 10 days of incubation; but the growth inhibition was studied for a total of 20 days. The complete time course is provided in Supplementary Fig. 5.

These findings demonstrate that lipopeptides from AMCV2 and FAU18 have strong and long-lasting antifungal activity.

To evaluate whether AMCV2 and FAU18 CLPs exhibited synergistic antifungal activity, both extracts were tested individually and in combination against *B. cinerea* 05.10 and *B. cinerea* T4 (Figs. 4C and 4D). After 5, 10 and 15 days of incubation, the inhibition zone produced by the combined treatment (10 µL AMCV2 + 10 µL FAU18) was comparable to those observed for the individual treatments with 20 µL of each extract. No enhancement of inhibition was detected, but importantly, no reduction in activity was observed either. These results indicate that lipopeptide extracts from AMCV2 and FAU18 possess similar inhibitory capacities and do not act synergistically.

Conidial germination assay

To gain deeper insight into the mechanisms underlying the biocontrol activity of the *Bacillus* lipopeptides, conidial germination assays were performed using *B. cinerea* B05.10 and *B. cinerea* T4. The results obtained for *B. cinerea* B05.10 are presented in Fig. 5, whereas those for *B. cinerea* T4 are provided in Supplementary Fig. 6. Conidia in both the untreated control and the methanol control germinated normally after 6 h, forming germ tubes of typical length. In contrast, conidia exposed to lipopeptides from AMCV2 and FAU18 exhibited a pronounced delay in germination, with most remaining ungerminated or developing only very short germ tubes at the same time point. To verify that these visual differences reflected a true inhibitory effect, the percentage of germinated conidia was statistically assessed (Fig. 6). This analysis confirmed a significant reduction in germination in the presence of lipopeptides compared with both controls ($p < 0.05$), whereas no significant differences were observed between untreated and methanol controls.

The inhibition of conidial germination (ICG%) was then calculated according to the equation described in the Materials and Methods section. The ICG values obtained when evaluating *B. cinerea* B05.10 conidial germination for FAU18 were 97.85 ± 6.83% relative to the untreated control and 98.20 ± 5.72% relative to the methanol control, while those for AMCV2 were 93.48 ± 4.97% and 92.98 ± 5.39%, respectively. The ICG values obtained when evaluating *B. cinerea* T4 conidial germination for FAU18 were 97.44 ± 8.10% relative to the untreated control and 97.84 ± 6.79% relative to the methanol control. For AMCV2 the values were 96.06 ± 12.61%

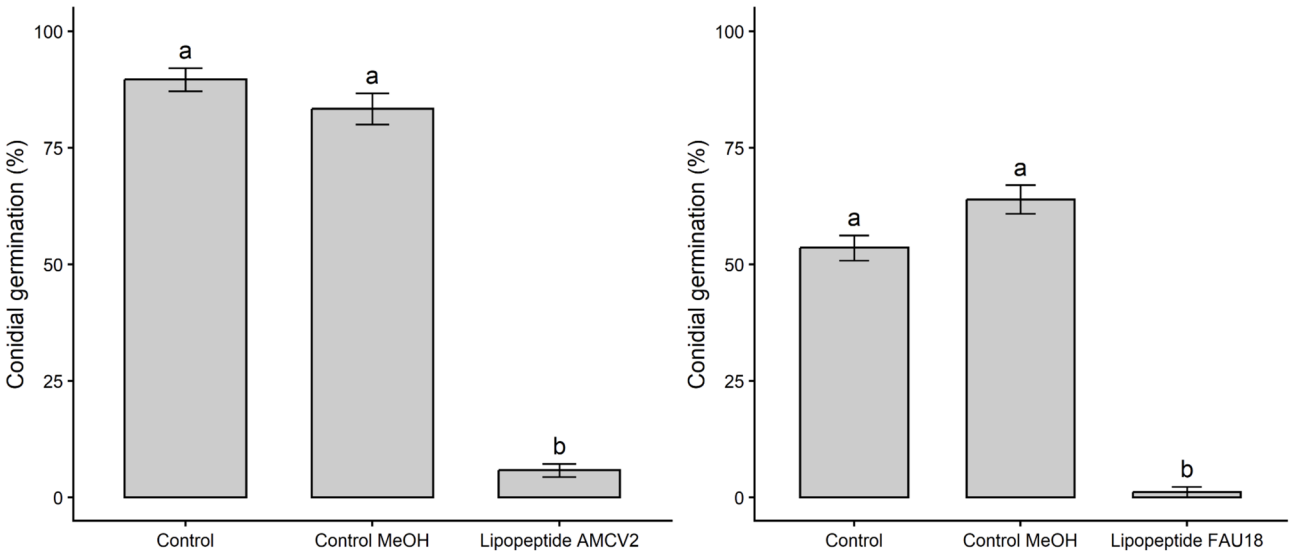

Fig. 6. Effect of *B. subtilis s.s.* AMCV2 and *B. subtilis s.s.* FAU18 derived lipopeptides on *Botrytis cinerea* B05.10 conidial germination. Conidial germination was evaluated after 6 h of incubation in untreated controls, methanol controls, and in the presence of lipopeptides produced by strains AMCV2 and FAU18. Bars represent the mean percentage of germinated conidia ± standard error (SE) calculated from 10 independent microscopic fields per treatment ($n = 10$). Different letters indicate statistically significant differences among treatments according to the Kruskal–Wallis test followed by Dunn's post hoc test with Benjamini–Hochberg correction ($p < 0.05$).

and 93.85 ± 19.77% respectively. The inclusion of both controls confirmed that methanol, used as the solvent for the lipopeptides, did not affect germination on its own. Therefore, the strong inhibitory effect observed can be attributed specifically to the lipopeptides, which effectively interfere with the early stages of *B. cinerea* development by preventing conidial germination.

Siderophore detection by CAS overlay assay

Siderophore biosynthetic clusters were consistently predicted in all five strains by AntiSMASH (bacillibactin in all five; petrobactin in TCT6, AMCV8, and FAU20). To validate these predictions experimentally, a CAS overlay assay (O-CAS) was performed, in which a modified CAS medium is added over pre-grown agar cultures. The O-CAS assay is a well-established method for detecting siderophore secretion, as the removal of iron from the CAS-dye complex produces a visible color change (orange/yellow halo) around bacterial colonies. AMCV8 produced a clear orange halo comparable to the positive control, confirming strong siderophore activity. TCT6 and FAU20 also generated halos, although these were notably less pronounced. By contrast, AMCV2 and FAU18 produced no visible halo. Overall, siderophore secretion was detectable only in strains belonging to the *B. cereus sensu lato* group under the tested conditions, despite siderophore biosynthetic clusters being predicted in all five genomes. We cannot rule out that they will be expressed and active under different conditions.

Concluding remarks

In this study, the integration of genomic and phenotypic analyses enabled the classification of the isolates into two species groups: *B. cereus sensu stricto* (FAU20, AMCV8, and TCT6) and *B. subtilis sensu stricto* (AMCV2 and FAU18). The taxonomic resolution of the *B. cereus* group proved challenging due to high genomic similarity and inconsistencies among available classification frameworks. Although the systems proposed by Carroll et al.[51] and Torres-Manno et al.[50] differ in their conceptual approaches, the incorporation of phenotypic evidence allowed for a consistent and reliable species assignment.

Genome mining revealed multiple biosynthetic gene clusters associated with secondary metabolites, including cyclic lipopeptides and siderophores. Notably, AMCV2 and FAU18 not only harbored CLP biosynthetic clusters but also produced bioactive compounds that inhibited *B. cinerea* strains B05.10 and T4. Microscopic analyses further indicated that CLPs interfered with conidial germination during early stages of development, contributing to their biocontrol activity.

In contrast, the *B. cereus sensu stricto* strains did not exhibit antifungal activity under the tested conditions, and despite their capacity to produce siderophores, their potential pathogenicity limits their applicability. Overall, AMCV2 and FAU18 emerge as effective and potentially safe candidates for the development of *Bacillus*-based biofungicides, supporting their prospective use in sustainable viticulture.

Materials and methods

Strains used in this study

Bacillus sp. AMCV2, AMCV8, FAU18, FAU20, TCT6 strains were isolated from the rhizosphere of commercial Malbec and Cabernet-Sauvignon vineyards across several Argentine wine producing regions during the 2016 harvest season[25]. The sequences of these strains were submitted to GenBank and registered under Bioproject ID PRJNA1390078.

Bacillus sp. strains were grown in liquid or solid Lysogeny broth (LB) medium at 28 °C[60]. The genomic sequences of *Bacillus* strains, used to perform comparative studies, were downloaded from the National Center for Biotechnology Information (NCBI) database (https://www.ncbi.nlm.nih.gov/), the accession numbers can be found in Supplementary Table S1. The fungal strains used in this study were *B. cinerea* B05.10 and *B. cinerea* T4[61].

Whole genome sequencing: assembly and annotation

Genomic DNA was extracted using the Gentra Puregene Yeast/Bact. Kit (QIAGEN) following the manufacturer's protocol for DNA purification of Gram-positive bacteria. The purity and integrity of the extracted DNA were assessed using a Nanodrop spectrophotometer and by agarose gel electrophoresis. The whole genome sequencing of the five *Bacillus* strains was performed on the Oxford Nanopore Technologies PromethION P2 Solo platform using an R10.4.1 flow cell (FLO-PRO114M). Libraries were prepared using the Rapid sequencing DNA V14 kit (SQK-RBK114.96), and raw data were basecalled using the super-accurate (SUP) model (Dorado v0.5.0). Nanopore reads were subsequently filtered using Filtlong (v0.2.0) and assembled with Flye (v2.9.1), followed by polishing using Medaka (v1.11.2) and reorientation via dnaapler resulting in a variable number of contigs across the samples. For TCT6, Illumina sequencing was also performed at SNPsaurus (Eugene, OR, USA) with an Illumina HiSeq 4000. The sequencing was carried out by means of Illumina paired-end libraries with 2 × 150-bp reads to reach ca. 60× read depth and a hybrid assembly was performed using Unicycler v0.5.1 on the Galaxy Australia server[32,62]. Oxford Nanopore sequencing datasets were evaluated using NanoPlot (NanoPack suite)[26] to assess read length distribution, total bases, and sequencing depth. Coverage was estimated by dividing the total number of sequenced bases by the assembled genome size for each strain.

Genomic annotation was performed using Prokka v1.14.6[27] also in Galaxy Australia. Additional annotation was conducted using the RAST server (RASTtk pipeline; accessed September 2024)[28], and eggNOG-mapper v2.1.12[29]. Custom scripts were used to generate the figures in this section with R version 4.3.1 (R Core Team, 2023) using the tidyverse and ggplot2 packages[63].

The presence of antibiotic resistance genes was assessed using ABRicate[64] in Galaxy Australia version 1.0.1. Prophage regions were predicted using the PHASTER (accessed December 2025)[35] and Phigaro (accessed December 2025)[36] algorithms and compared using BLASTn (accessed December 2025)[65]. Insertion sequences

(IS) were identified with ISEScan in Galaxy Europe version 1.7.3[33] using the default parameters. The distribution and genomic context of insertion sequences (IS) were further analyzed using ISCompare v1.0.5a[34].

Plant growth–promoting traits (PGPTs) were predicted using PLaBAse PGPT-Pred v1.02[37], an ontology-based framework for the identification of PGPT-associated protein-coding genes based on curated BLASTp and HMM profiles.

A targeted search for phytohormone-associated genes was performed to identify sequences related to auxin biosynthesis (*ipdC*, *aldH*, *ysnE*, *iaaM*, *iaaH*)[38,39], cytokinin metabolism[43] and biosynthesis (*ipt*, *miaA*, *log/yvdD*)[43], gibberellin biosynthetic operon genes (*cps*, *ks*, *cyp112*, *cyp114*, *cyp117*)[44], and *acdS* encoding ACC deaminase[45].

KEGG Orthology assignments were obtained using GhostKOALA v3.1[40], and pathway reconstruction was performed using the KEGG Mapper Reconstruct tool (accessed February 2026)[41,42] to evaluate the completeness of the phytohormone biosynthetic pathways.

Phylogenetic analysis

A phylogenetic analysis was performed using the assembled and annotated genomes. Taxonomic classification was carried out with BTyper3 version 3.4.0[46]. In addition to taxonomic classification, genome-based classification and biosafety assessment of strains belonging to the *B. cereus* group were performed with BTyper3 to screen the genomes for the presence of virulence and toxin associated genetic markers. Specifically, the analysis included detection of *B. anthracis* virulence genes, genes encoding toxins characteristic of *B. thuringiensis* and markers associated with foodborne pathogenicity. This integrated approach allowed simultaneous evaluation of taxonomic affiliation and potential biosafety risks associated with pathogenic or toxigenic members of the *B. cereus* group.

Additionally, average nucleotide identity (ANI) was calculated using Jspecies (accessed August 2025)[47], and the digital DNA: DNA hybridization (DDH) was estimated through the TYGS server (accessed September 2024)[48]. The heatmaps were generated using an in-house python script. See Supplementary Table S1 for the NCBI accession numbers of the *Bacillus* sequences downloaded.

Core genome alignments were generated using Roary v3.13.0[66], and maximum-likelihood phylogenetic trees were then constructed with FastTree v2.1.10[67] both in Galaxy Australia. The resulting phylogenetic trees were visualized with iTOL (Interactive Tree of Life) (accessed October 2025)[68]. To evaluate the evolutionary relationships of AMCV2 and FAU18, representative strains were selected from the *B. subtilis* group.

Phase-contrast microscopy for the detection of parasporal inclusions

Fresh preparations from sporulated bacterial cultures were examined by phase-contrast microscopy to evaluate cellular morphology. Observations were carried out using a Nikon Eclipse E200 binocular microscope equipped with a 100× oil immersion objective[69].

Secondary metabolite profiling for biocontrol potential

Biosynthetic gene clusters (BGCs) related to secondary metabolite production were identified from the genomic sequences of the *Bacillus* strains using antiSMASH version 7.0[70].

Comparative analysis of biosynthetic gene clusters of interest

A few biosynthetic gene clusters (BGCs) predicted by antiSMASH were selected for comparative analysis based on their high similarity to known compounds, including bacillibactin (all five strains), petrobactin (TCT6, AMCV8, and FAU20), and fengycin (AMCV2 and FAU18). For each selected cluster, the corresponding genomic regions were compared at the protein level using BLASTp[65] to evaluate amino acid identity and query coverage among homologous genes. Synteny analysis was performed to assess gene content, order, and orientation within each cluster using the Clinker/CAGECAT pipeline v1.0[59].

Isolation and antifungal activity of cyclic lipopeptides

For cyclic lipopeptides (CLPs) isolation, the *Bacillus* strains were grown in MOLP media[71]. Cell-free culture supernatants were acidified with 12 N HCl to pH 2.0 and incubated overnight at 4 °C to allow precipitation[71–73]. The resulting precipitates were collected by centrifugation, resuspended in 100% methanol, and stored at − 20 °C until use.

The antifungal activity of the isolated CLPs was evaluated using the paper disc diffusion method. Sterile filter paper discs were impregnated with 20 µL of each methanol resuspended extract. A methanol impregnated disc was included as a negative control. Plates containing 20 mL of potato dextrose agar (PDA) (200 g/L Potato infusion, 20 g/L glucose, 15 g/L agar, pH 5.6 ± 0.2) were inoculated with a 6-mm plug of actively growing *B. cinerea* B05.10 *or B. cinerea* T4 and placed in the center, and the discs were positioned equidistantly at ~ 3 cm from the plug. Plates were incubated at 23 °C, and inhibition zones were recorded on day 5, day 10, day 15 and day 20.

To evaluate potential synergistic effects between AMCV2 and FAU18 CLPs, a mycelial plug of *B. cinerea* T4 or 05.10 (5 mm diameter) was placed at the center of a PDA Petri dish. Four sterile filter paper discs were positioned equidistantly at ~ 3 cm from the plug. Each disc was impregnated with one of the following treatments: 20 µL of AMCV2 extract, 20 µL of FAU18 extract, 20 µL of methanol (negative control), or a mixture of 10 µL AMCV2 extract + 10 µL FAU18 extract. Plates were incubated at 23 °C, and inhibition zones were monitored after 10 and 20 days of incubation.

Conidial germination assays

To determine the effect of the CLPs produced by the bacterial strains on conidial germination, assays were performed on microscope slides coated with a thin layer of commercial Potato Dextrose Broth (PDB) prepared at 0.5%. On each thin medium layer, three drops of 10 µL of the conidial suspension were placed at evenly spaced positions. The first drop was left untreated as a negative control, the second drop was supplemented with 10 µL of methanol, and the third drop received 10 µL of the lipopeptide solution to be tested. The slides were placed inside Petri dishes, which contained sterile paper moistened with sterile bidestilated water. The Petri dishes were incubated at 23 °C for 6 hs. Conidial germination was observed using a light microscope. A conidium was considered germinated when the germ tube length was at least twice the conidial diameter. The conidial germination percentage was determined by counting germinated and non-germinated conidia across 10 randomly selected microscopic fields (40× objective, 10× ocular) for each treatment and calculating the proportion of germinated conidia relative to the total observed, following the method described by Chakraborty et al.[74]. Statistical analyses were performed in R (v4.3.1) using the Kruskal-Wallis test followed by Dunn's post hoc test with Benjamini-Hochberg correction ($p < 0.05$), and plots were generated using an in-house R script.

The percentage of inhibition of conidial germination (± standard error) was calculated from mean values as follows:

$$\mathrm{ICG\%} = (\mathrm{C} - \frac{T}{C}) \times 100 \quad (1)$$

where ICG = inhibition of conidial germination, C = percentage of germinated conidia in the control, and T = percentage of germinated conidia in the treatment.

Siderophore detection by CAS overlay assay

Siderophore production was evaluated using the CAS overlay method[75]. Bacterial strains were spot-inoculated (2.5 µL of a 10^6 CFU/mL suspension) onto R_2A agar plates (0.5 g/L yeast extract, 0.5 g/L peptone, 0.5 g/L casamino acids, 0.5 g/L glucose, 0.5 g/L soluble starch, 0.3 g/L sodium pyruvate, 0.3 g/L dipotassium phosphate, 0.05 g/L magnesium sulfate, and 15 g/L agar; pH adjusted to 6.5 with KOH) and incubated at 28 °C in the dark for 48 h. After incubation, a second layer of Chrome Azurol S (CAS) medium was poured onto the plates, prepared by mixing 15 mL of overlay solution (33.3 g/L PIPES buffer in distilled water, adjusted to pH 6.8 with KOH, supplemented with 10 g/L agarose; sterilized by autoclaving and cooled to ~ 50 °C) with 5 mL of CAS indicator solution (0.06 g CAS dye dissolved in 50 mL distilled water, combined with 10 mL of 10 mM HCl containing 3 mg $FeCl_3 \cdot 6\ H_2O$, and 7 mg HDTMA dissolved in 40 mL distilled water). Plates were allowed to rest at room temperature for 24 h before evaluation. The appearance of an orange/yellow halo around colonies was considered indicative of siderophore production. *Pantoea agglomerans* NMR14 known to produce siderophores[25] was used as a positive control.

Data availability

Data generated in this research are provided as supplementary material with this manuscript. DNA sequence data are deposited in the NCBI GenBank database under Bioproject ID PRJNA1390078.

Received: 9 January 2026; Accepted: 12 March 2026
Published online: 27 March 2026

References

1. Mozell, M. R. & Thach, L. The impact of climate change on the global wine industry: Challenges & solutions. *Wine Econ. Policy.* **3**, 81–89 (2014).
2. OIV. *State Of The World Vine And Wine Sector In 2023*. (2024). Available at https://www.oiv.int/sites/default/files/2024-04/OIV_STATE_OF_THE_WORLD_VINE_AND_WINE_SECTOR_IN_2023.pdf
3. Elad, Y., Vivier, M. & Fillinger, S. *Botrytis*, the good, the bad and the ugly. In *Botrytis - The Fungus, the Pathogen and its Management in Agricultural Systems* 1–15 (Springer International Publishing, 2015).
4. Fekete, É. et al. Genetic diversity of a *Botrytis cinerea* cryptic species complex in Hungary. *Microbiol. Res.* **167**, 283–291 (2012).
5. Ky, I. et al. Assessment of grey mould (*Botrytis cinerea*) impact on phenolic and sensory quality of Bordeaux grapes, musts and wines for two consecutive vintages. *Aust J. Grape Wine Res.* **18**, 215–226 (2012).
6. Steel, C. C., Blackman, J. W. & Schmidtke, L. M. Grapevine bunch rots: Impacts on wine composition, quality, and potential procedures for the removal of wine faults. *J. Agric. Food Chem.* **61**, 5189–5206 (2013).
7. Pertot, I. et al. Combining biocontrol agents with different mechanisms of action in a strategy to control *Botrytis cinerea* on grapevine. *Crop Prot.* **97**, 85–93 (2017).
8. Rotolo, C. et al. Use of biocontrol agents and botanicals in integrated management of *Botrytis cinerea* in table grape vineyards. *Pest Manag Sci.* **74**, 715–725 (2018).
9. Sharma, R. R., Singh, D. & Singh, R. Biological control of postharvest diseases of fruits and vegetables by microbial antagonists: A review. *Biol. Control.* **50**, 205–221 (2009).
10. Calvo-Garrido, C. et al. Microbial antagonism toward *Botrytis* bunch rot of grapes in multiple field tests using one *Bacillus ginsengihumi* strain and formulated biological control products. *Front. Plant. Sci.* **10**, 1133 (2019).
11. Briz-Cid, N., Castro-Sobrino, L., Rial-Otero, R., Cancho-Grande, B. & Simal-Gándara, J. Fungicide residues affect the sensory properties and flavonoid composition of red wine. *J. Food Compos. Anal.* **66**, 185–192 (2018).
12. Esteve-Turrillas, F. A., Agulló, C., Abad-Somovilla, A. & Mercader, J. V. Abad-Fuentes, A. Fungicide multiresidue monitoring in international wines by immunoassays. *Food Chem.* **196**, 1279–1286 (2016).
13. Borriss, R. *Bacillus*. In Beneficial Microbes in Agro-Ecology: Bacteria and Fungi (eds Amaresan, N., Senthil Kumar, M., Annapurna, K., Kumar, K. & Sankaranarayanan, A.) 107–132 (Elsevier, 2020).
14. Fira, D., Dimkić, I., Berić, T., Lozo, J. & Stanković, S. Biological control of plant pathogens by *Bacillus* species. *J. Biotechnol.* **285**, 44–55 (2018).

15. Yuan, S. et al. Biocontrol Capabilities of *Bacillus subtilis E11* against Aspergillus flavus In Vitro and for Dried Red Chili (*Capsicum annuum L*). *Toxins (Basel)*. **15**, 308 (2023).
16. Grahovac, J., Pajčin, I. & Vlajkov, V. *Bacillus* VOCs in the Context of Biological Control. *Antibiotics* **12**, 581 (2023).
17. Zhao, H. et al. Biological activity of lipopeptides from *Bacillus*. *Appl. Microbiol. Biotechnol.* **101**, 5951–5960 (2017).
18. Carroll, L. M., Cheng, R. A., Wiedmann, M. & Kovac, J. Keeping up with the *Bacillus cereus* group: taxonomy through the genomics era and beyond. *Crit. Rev. Food Sci. Nutr.* **62**, 7677–7702 (2022).
19. Bottone, E. J. *Bacillus cereus*, a volatile human pathogen. *Clin. Microbiol. Rev.* **23**, 382–398 (2010).
20. Stenfors Arnesen, L. P., Fagerlund, A. & Granum, P. E. From soil to gut: *Bacillus cereus* and its food poisoning toxins. *FEMS Microbiol. Rev.* **32**, 579–606 (2008).
21. Edwards, K. A., Clancy, H. A. & Baeumner, A. J. Bacillus anthracis: toxicology, epidemiology and current rapid-detection methods. *Anal. Bioanal. Chem 2005 384:1* **384**, 73–84 (2005).
22. Hoffmaster, A. R., Fitzgerald, C. C., Ribot, E., Mayer, L. W. & Popovic, T. Molecular Subtyping of *Bacillus anthracis* and the 2001 Bioterrorism-Associated Anthrax Outbreak. *Emerg. Infect. Dis.* **8**, 1111–1116 (2002).
23. Kumar, P., Kamle, M., Borah, R., Mahato, D. K. & Sharma, B. *Bacillus thuringiensis* as microbial biopesticide: uses and application for sustainable agriculture. *Egypt. J. Biol. Pest Control.* **31**, 1–7 (2021).
24. Blanco Crivelli, X., Cundon, C., Bonino, M. P., Sanin, M. S. & Bentancor, A. The Complex and Changing Genus Bacillus: A Diverse Bacterial Powerhouse for Many Applications. *Bacteria* **3**, 256–270 (2024).
25. Oyuela Aguilar, M. et al. Screening of epiphytic rhizosphere-associated bacteria in argentinian malbec and cabernet-sauvignon vineyards for potential use as biological fertilisers and pathogen-control agents. *Oeno One.* **55**, 145–157 (2021).
26. De Coster, W., D'Hert, S., Schultz, D. T., Cruts, M. & Van Broeckhoven, C. NanoPack: visualizing and processing long-read sequencing data. *Bioinformatics* **34**, 2666–2669 (2018).
27. Seemann, T. & Prokka Rapid prokaryotic genome annotation. *Bioinformatics* **30**, 2068–2069 (2014).
28. Aziz, R. K. et al. The RAST Server: Rapid annotations using subsystems technology. *BMC Genom.* **9**, 75 (2008).
29. Cantalapiedra, C. P., Hernandez-Plaza, A., Letunic, I., Bork, P. & Huerta-Cepas J. eggNOG-mapper v2: Functional Annotation, Orthology Assignments, and Domain Prediction at the Metagenomic Scale. *Mol. Biol. Evol.* **38**, 5825–5829 (2021).
30. Moshe, M. et al. Comparative genomics of *Bacillus cereus sensu lato* spp. biocontrol strains in correlation to in-vitro phenotypes and plant pathogen antagonistic capacity. *Front. Microbiol.* **14**, 996287 (2023).
31. Wang, T., Shi, Y., Zheng, M. & Zheng, J. Comparative Genomics Unveils Functional Diversity, Pangenome Openness, and Underlying Biological Drivers among *Bacillus subtilis* Group. *Microorganisms* **12**, 986 (2024).
32. Afgan, E. et al. The Galaxy platform for accessible, reproducible and collaborative biomedical analyses: 2022 update. *Nucleic Acids Res.* **50**, W345–W351 (2022).
33. Xie, Z. & Tang, H. ISEScan: automated identification of insertion sequence elements in prokaryotic genomes. *Bioinformatics* **33**, 3340–3347 (2017).
34. Mogro, E. G., Ambrosis, N. M. & Lozano, M. J. Easy identification of insertion sequence mobilization events in related bacterial strains with ISCompare. *G3 Genes|Genomes|Genetics* **11**, (2021).
35. Arndt, D. et al. PHASTER: a better, faster version of the PHAST phage search tool. *Nucleic Acids Res.* **44**, W16–W21 (2016).
36. Starikova, E. V. et al. Phigaro: high-throughput prophage sequence annotation. *Bioinformatics* **36**, 3882–3884 (2020).
37. Patz, S. et al. PLaBAse: A comprehensive web resource for analyzing the plant growth-promoting potential of plant-associated bacteria. *bioRxiv* https://doi.org/10.1101/2021.12.13.472471 (2021).
38. Tang, J. et al. Biosynthetic Pathways and Functions of Indole-3-Acetic Acid in Microorganisms. *Microorganisms* **11**, 2077(2023).
39. Shao, J. et al. Participating mechanism of a major contributing gene *ysnE* for auxin biosynthesis in *Bacillus amyloliquefaciens* SQR9. *J. Basic. Microbiol.* **61**, 569–575 (2021).
40. Kanehisa, M., Sato, Y. & Morishima, K. BlastKOALA and GhostKOALA: KEGG Tools for Functional Characterization of Genome and Metagenome Sequences. *J. Mol. Biol.* **428**, 726–731 (2016).
41. Kanehisa, M. & Sato, Y. KEGG Mapper for inferring cellular functions from protein sequences. *Protein Sci.* **29**, 28–35 (2020).
42. Kanehisa, M., Sato, Y. & Kawashima, M. KEGG mapping tools for uncovering hidden features in biological data. *Protein Sci.* **31**, 47–53 (2022).
43. Frébortová, J. & Frébort, I. Biochemical and Structural Aspects of Cytokinin Biosynthesis and Degradation in Bacteria. *Microorganisms* **9**, 1314 (2021).
44. Nett, R. S. et al. Elucidation of gibberellin biosynthesis in bacteria reveals convergent evolution. *Nat. Chem. Biol.* **13**, 69 (2016).
45. Glick, B. R. Bacteria with ACC deaminase can promote plant growth and help to feed the world. *Microbiol. Res.* **169**, 30–39 (2014).
46. Carroll, L. M., Cheng, R. A. & Kovac, J. No Assembly Required: Using BTyper3 to Assess the Congruency of a Proposed Taxonomic Framework for the *Bacillus cereus* Group With Historical Typing Methods. *Front Microbiol* **11**:580691, (2020).
47. Richter, M., Rosselló-Móra, R., Glöckner, O., Peplies, J. & F. & JSpeciesWS: A web server for prokaryotic species circumscription based on pairwise genome comparison. *Bioinformatics* **32**, 929–931 (2016).
48. Meier-Kolthoff, J. P. & Göker, M. TYGS is an automated high-throughput platform for state-of-the-art genome-based taxonomy. *Nat Commun* **10,** 2182, (2019).
49. Medeot, D. B., Fernandez, M., Morales, G. M. & Jofré, E. Fengycins From *Bacillus amyloliquefaciens* MEP218 Exhibit Antibacterial Activity by Producing Alterations on the Cell Surface of the Pathogens *Xanthomonas axonopodis pv. vesicatoria* and *Pseudomonas aeruginosa* PA01. *Front Microbiol* **10**, 3107 (2020).
50. Torres Manno, M. A., Repizo, G. D., Magni, C., Dunlap, C. A. & Espariz, M. The assessment of leading traits in the taxonomy of the Bacillus cereus group. *Antonie van Leeuwenhoek Int. J. Gen. Mol. Microbiol.* **113**, 2223–2242 (2020).
51. Carroll, L. M., Wiedmann, M. & Kovac, J. Proposal of a Taxonomic Nomenclature for the *Bacillus cereus* Group Which Reconciles Genomic Definitions of Bacterial Species with Clinical and Industrial Phenotypes. (2020). https://doi.org/10.1128/mBio
52. Yousten, A. A. & Rogoff, M. H. Metabolism of *Bacillus thuringiensis* in relation to spore and crystal formation. *J. Bacteriol.* **100**, 1229–1236 (1969).
53. Nifakos, K. et al. Genomic analysis and secondary metabolites production of the endophytic *Bacillus velezensis* bvel1: A biocontrol agent against *Botrytis cinerea* causing bunch rot in post-harvest table grapes. *Plants* **10**, 1716 (2021).
54. Dimopoulou, A. et al. Direct Antibiotic Activity of Bacillibactin Broadens the Biocontrol Range of *Bacillus amyloliquefaciens* MBI600. *mSphere* **6**, (2021).
55. Hayrapetyan, H., Siezen, R., Abee, T. & Groot, M. N. Comparative genomics of iron-transporting systems in *Bacillus cereus* strains and impact of iron sources on growth and biofilm formation. *Front. Microbiol.* **7**, 194609 (2016).
56. Valenzuela Ruiz, V. et al. Regulation, Biosynthesis, and Extraction of Bacillus-Derived Lipopeptides and Its Implications in Biological Control of Phytopathogens. *Stresses* **4**, 107–132 (2024).
57. Ongena, M. & Jacques Bacillus lipopeptides: versatile weapons for plant disease biocontrol. *Trends Microbiol.* **16**, 115–125 (2008).
58. Cawoy, H. et al. Lipopeptides as main ingredients for inhibition of fungal phytopathogens by Bacillus subtilis/amyloliquefaciens. *Microb. Biotechnol.* **8**, 281–295 (2015).
59. van den Belt, M. et al. CAGECAT: The CompArative GEne Cluster Analysis Toolbox for rapid search and visualization of homologous gene clusters. *BMC Bioinform.* **24**, 181 (2023).
60. Bertani, G. Studies on Lysogenesis I. *J. Bacteriol.* **62**, 293–300 (1951).
61. Staats, M. & van Kan, J. A. L. Genome update of *Botrytis cinerea* strains B05.10 and T4. *Eukaryot. Cell.* **11**, 1413–1414 (2012).

62. Wick, R. R., Judd, L. M., Gorrie, C. L. & Holt, K. E. Unicycler: Resolving bacterial genome assemblies from short and long sequencing reads. *PLoS Comput. Biol* **13**, e1005595 (2017).
63. Wickham, H. ggplot2: Elegant Graphics for Data Analysis. *Springer* 189–201 (2016).
64. Seemann, T. & ABRicate Mass Screening of Contigs for Antibiotic Resistance Genes. (2016). https://github.com/tseemann/abricate
65. Altschul, S. F., Gish, W., Miller, W., Myers, E. W. & Lipman, D. J. Basic local alignment search tool. *J. Mol. Biol.* **215**, 403–410 (1990).
66. Page, A. J. et al. Roary: Rapid large-scale prokaryote pan genome analysis. *Bioinformatics* **31**, 3691–3693 (2015).
67. Price, M. N., Dehal, P. S. & Arkin, A. P. FastTree 2 – Approximately Maximum-Likelihood Trees for Large Alignments. *PLoS One*. **5**, e9490 (2010).
68. Letunic, I. & Bork, P. Interactive tree of life (iTOL) v5: An online tool for phylogenetic tree display and annotation. *Nucleic Acids Res.* **49**, W293–W296 (2021).
69. Pérez, M. P., Sauka, D. H., Onco, M. I., Berretta, M. F. & Benintende, G. B. Selection of *Bacillus thuringiensis* strains toxic to cotton boll weevil (Anthonomus grandis, Coleoptera: Curculionidae) larvae. *Rev. Argent. Microbiol.* **49**, 264–272 (2017).
70. Blin, K. et al. antiSMASH 7.0: new and improved predictions for detection, regulation, chemical structures and visualisation. *Nucleic Acids Res.* **51**, W46–W50 (2023).
71. Medeot, D. B. et al. Improvement of biomass and cyclic lipopeptides production in *Bacillus amyloliquefaciens* MEP218 by modifying carbon and nitrogen sources and ratios of the culture media. *Biol. Control*. **115**, 119–128 (2017).
72. Kim, P. I. et al. Purification and characterization of a lipopeptide produced by *Bacillus thuringiensis* CMB26. *J. Appl. Microbiol.* **97**, 942–949 (2004).
73. Vater, J. et al. Matrix-Assisted Laser Desorption Ionization-Time of Flight Mass Spectrometry of Lipopeptide Biosurfactants in Whole Cells and Culture Filtrates of *Bacillus subtilis* C-1 Isolated from Petroleum Sludge. *Appl. Environ. Microbiol.* **68**, 6210 (2002).
74. Chakraborty, M. et al. Inhibitory Effects of Linear Lipopeptides From a Marine *Bacillus subtilis* on the Wheat Blast Fungus *Magnaporthe oryzae Triticum*. *Front. Microbiol.* **11**, 527783 (2020).
75. Pérez-Miranda, S., Cabirol, N., George-Téllez, R., Zamudio-Rivera, L. S. & Fernández, F. J. O-CAS, a fast and universal method for siderophore detection. *J. Microbiol. Methods*. **70**, 127–131 (2007).

Acknowledgements

D.M.L. is fellow of ANPCyT, C.R., R.R.W. and J.F.N. are fellows of CONICET. D.S., E.J. and M.P are members of the Research Career of CONICET.

Author contributions

D.M.L. conceived the study, conducted the experiments, performed the bioinformatics and statistical analyses, and wrote the manuscript. R.R.W. and C.R. assisted with the bioinformatics analysis. A.M.D. and L.H.H. performed DNA sequencing. D.S. performed microscopy analyses. J.F.N., A.M.T., and E.J. contributed to manuscript review. M.P. conceived the study, supervised the study, analyzed the data and served as the corresponding author. All authors reviewed the manuscript, contributed to the discussion, and approved the final version.

Funding

This work was supported by the Consejo Nacional de Investigaciones Científicas y Técnicas (CONICET, Argentina) Grant/Award PIP2022-0367 and Agencia Nacional de Promoción Científica y Tecnológica (ANPCyT, Argentina) PICT2021-0277 to M.P.

Declarations

Competing interests

The authors declare no competing interests.

Additional information

Supplementary Information The online version contains supplementary material available at https://doi.org/10.1038/s41598-026-44555-9.

Correspondence and requests for materials should be addressed to M.P.

Reprints and permissions information is available at www.nature.com/reprints.

Publisher's note Springer Nature remains neutral with regard to jurisdictional claims in published maps and institutional affiliations.